

ETH-TH/97-21
GEF-TH-8/1997
hep-ph/9707345

JET PHOTOPRODUCTION AT HERA

Stefano FRIXIONE¹

Theoretical Physics, ETH, Zurich, Switzerland

Giovanni RIDOLFI

INFN, Sezione di Genova, Genoa, Italy

Abstract

We compute various kinematical distributions for one-jet and two-jet inclusive photoproduction at HERA. Our results are accurate to next-to-leading order in QCD. We use the subtraction method for the cancellation of infrared singularities. We perform a thorough study of the reliability of QCD predictions; in particular, we consider the scale dependence of our results and discuss the cases when the perturbative expansion might break down. We also deal with the problem of the experimental definition of the pointlike and hadronic components of the incident photon, and briefly discuss the sensitivity of QCD predictions upon the input parameters of the calculation, like α_s and the parton densities.

¹Work supported by the Swiss National Foundation.

1. Introduction

Jet production is a frequent phenomenon in high-energy collisions. It is characterized by large rates, which allow measurements of its kinematical features even in the case of high jet multiplicity (like six-jet events at Tevatron and five-jet events at LEP). Complete next-to-leading order QCD calculations are available for one- and two-jet inclusive quantities in hadronic collisions [1], and up to four-jet inclusive quantities in e^+e^- collisions [2]. The typical energy scale for the hard process is of the order of the average jet transverse momentum; at presently operating colliders, this means that the hard production process takes place in an energy domain where the predictions of perturbative QCD are particularly accurate.

At hadron colliders, for one- and two-jet inclusive observables the uncertainty affecting the theoretical results is smaller than experimental errors, and stringent tests for QCD can be carried out. Although most of the comparisons between theory and data are quite successful, some issues need to be better clarified. In particular, we recall that the CDF collaboration reports [3] an excess of events in the tail of the E_T distribution with respect to the theoretical predictions (this discrepancy, however, can be absorbed in a suitable modification of the parton densities [4]), and that the comparison between data [5] taken at different center-of-mass energies in $p\bar{p}$ collisions is still not consistent with the scaling found in QCD.

The amount of experimental information relevant for lepton-hadron collisions is presently not as detailed as in the case of hadronic or e^+e^- processes. Nevertheless, in the near future the increased luminosity of the HERA collider will allow a statistically significant study also for this kind of hard scattering. In jet production at HERA, one can consider two different kinematical regimes. In one class of events, the electron is scattered at large angles (deep inelastic scattering). In another class of events, the electron is lost in the beam-pipe (or tagged at very small angles); in this case, it acts as a source of real photons, which eventually interact with the partons in the proton beam. It is well known that an on-shell photon has a finite probability of fluctuating into a hadronic state before undergoing a hard collision. Therefore, for a comparison with experimental data on jet photoproduction, one must consider QCD processes in which the photon directly enters the hard parton scattering, and processes in which the photon emits partons (in a way parametrized by some universal but non-calculable parton densities) which enter the hard parton scattering.

Partial next-to-leading order QCD results for jet photoproduction have been available for some time [6]. Complete calculations for one-jet and two-jet inclusive quantities which include the contributions of all the relevant partonic subprocesses have been reported in refs. [7-9]. Comparison with data are encouraging (see for example refs. [10,11] for a recent review on this point), but larger statistics is needed in order to study more exclusive quantities and to fully test the predictions of the theory. Therefore, the aim of this paper is not to perform a comparison with existing data, but rather to discuss some general features of the theoretical predictions of jet photoproduction in the HERA energy range. Our predictions are obtained using the computer codes ² recently presented in ref. [9], and are based on the general formalism of ref. [12]. The fundamental difference between the results of refs. [7,8] and those presented here is that the former are obtained in the framework of the slicing method, while the latter rely upon the subtraction method. Both methods have been devised in order to cancel analytically the infrared divergencies which arise in the intermediate steps of any next-to-leading order QCD calculation. The slicing method requires the matrix elements for the real emission processes to be approximated in those regions of the phase space which are close to an infrared (soft or collinear) singularity. These regions are defined by means of some non-physical parameters. Physical results must be independent of these parameters; it is in general a non-trivial task to prove (numerically) that this is indeed the case, at the required level of accuracy. Notice also that in principle this proof has to be carried out for each observable, since different quantities may display different convergence properties. In the subtraction method, the exact expression of the matrix elements is used in the whole phase space. The main advantage of this method is that it does *not* require the introduction of any non-physical parameter. In the following, we will encounter cases where this feature of the subtraction method will turn out to be advantageous in the calculation of physical quantities.

This paper is organized as follows. In section 2 we study the problem of the reliability of the next-to-leading order QCD predictions for jet observables at HERA, where the typical transverse momenta are sizeably smaller than in the case of hadron collider experiments. We consider several one-jet and two-jet inclusive quantities, and we isolate the regions where QCD perturbative expansion breaks down, and an all-order resummation of soft-gluon effects is mandatory. We also discuss the prob-

²The codes, which return parton kinematical configurations with an appropriate weight, are available upon request.

lem of the *operational* separation of the pointlike (or direct) and of the hadronic (or resolved) components of the cross section. In section 3 we present some predictions for quantities whose measurement would help the understanding of the jet production mechanism and ultimately to better test QCD in the context of photon-hadron collisions. Finally, in section 4 we report our conclusions.

2. General features of QCD predictions

Any production cross section in electron-proton collisions is dominated by the exchange of low-virtuality photons. The electron behaves therefore as a broad-band beam of real photons, whose momenta are distributed according to the Weizsäcker-Williams function [13]

$$f_{\gamma}^{(e)}(y) = \frac{\alpha_{\text{em}}}{2\pi} \left[\frac{1 + (1-y)^2}{y} \log \frac{Q^2(1-y)}{m_e^2 y^2} + 2m_e^2 y \left(\frac{1}{Q^2} - \frac{1-y}{m_e^2 y^2} \right) \right], \quad (2.1)$$

where m_e is the electron mass and y is the fraction of the electron longitudinal momentum carried by the photon. Notice that in eq. (2.1) terms which are non-singular for $m_e \rightarrow 0$ cannot be neglected in the HERA energy range, because of the $1/y$ singularity [14,15]. The quantity Q must be taken to be the minimum between the typical energy scale which characterizes the production process, and the upper limit of the absolute value of the photon virtuality (see ref. [15] for a detailed discussion of this point). The cross section for a generic electron-proton scattering process is given by

$$d\sigma_{ep}(K_e, K_p) = \int_{y_{\min}}^{y_{\max}} dy f_{\gamma}^{(e)}(y) d\sigma_{\gamma p}(yK_e, K_p), \quad (2.2)$$

where K_e and K_p are the momenta of the incoming electron and proton respectively, and $0 < y_{\min} < y_{\max} \leq 1$ are fixed by kinematical boundary conditions or experimental cuts. The relevant hard scattering quantity is therefore the cross section for photon-proton collisions, $d\sigma_{\gamma p}$. Since the HERA experiments can measure the momentum of the scattered electron down to very small values of the scattering angle, it is possible, in principle, to measure directly $d\sigma_{\gamma p}$ for a fixed value of the photon energy (with the current electron and proton energies, $E_e = 27.5$ GeV and $E_p = 820$ GeV, the accessible range in the photon-proton center-of-mass energy is at best $100 \text{ GeV} \leq E_{cm}(\gamma p) \leq 280 \text{ GeV}$).

The possibility of measuring the photon-proton jet cross section for several different center-of-mass energies would be an interesting test of the scaling laws predicted

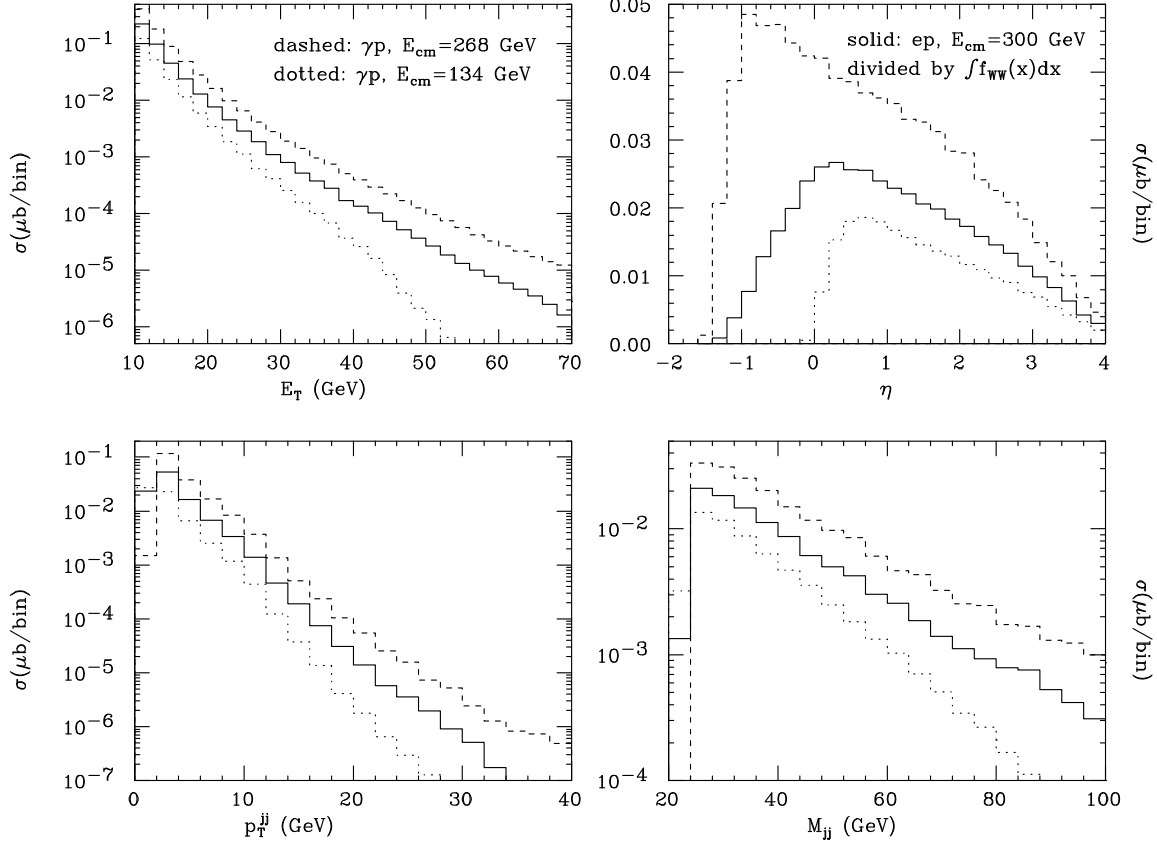


Figure 1: *Comparison between monoenergetic photon-proton and electron-proton (Weizsäcker-Williams approximation) cross sections, for various jet distributions.*

by QCD. For this reason, we have studied the energy dependence of differential jet distributions in monoenergetic photon-proton collisions, comparing them with the same quantities obtained in electron-proton collisions in the Weizsäcker-Williams approximation, eq. (2.2). The results, obtained at NLO in QCD, are shown in fig. 1. In the two upper plots we present single-inclusive distributions in the transverse energy E_T of the jet and in its pseudorapidity η for $E_T > E_T^{\text{cut}}$, $E_T^{\text{cut}} = 10$ GeV. In the two lower plots, we show the distributions in the transverse momentum, p_T^{jj} , and invariant mass, M_{jj} , of the pair of the two hardest jets in the event. In this case, we require the transverse energies of the two observed jets to satisfy the constraints $E_{1T} > E_{1T}^{\text{cut}}$, $E_{2T} > E_{2T}^{\text{cut}}$, with $E_{1T}^{\text{cut}} = E_{2T}^{\text{cut}} = 10$ GeV (the fact that the same value of the transverse energy cut is used for both jets will be discussed below in detail). Jets are defined by

the cone algorithm [16] with opening angle $R = 1$. We used the sets MRSA' [17] and GRV-HO [18] for parton densities in the proton and the photon respectively. The renormalization and factorization scales have been chosen equal to half the transverse energy of the event; from now on, this choice will be our default and will be denoted as μ_0 . Λ_{QCD} has been set equal to the value suggested by the MRSA' parton densities, $\Lambda_5^{\overline{\text{MS}}} = 152$ MeV. Each distribution in fig. 1 is presented for two different energies of the photon-proton system, 134 GeV (dotted curves) and 268 GeV (dashed curves), which correspond to $y = 0.2$ and $y = 0.8$ in eq. (2.2) respectively. The solid curves show the predictions for electron-proton collisions at $E_{cm}(ep) = 300$ GeV in the Weizsäcker-Williams approximation, eq. (2.2), with $y_{min} = 0.2$, $y_{max} = 0.8$, and $Q^2 = 4$ GeV², rescaled by a factor

$$\left[\int_{y_{min}}^{y_{max}} f_{\gamma}^{(e)}(y) dy \right]^{-1} \simeq 26.9. \quad (2.3)$$

The difference in normalization between the curves relevant for the two photon-proton center-of-mass energies is sizeable. Phase-space effects are clearly visible in the tail of the E_T , p_T^{jj} and M_{jj} distributions, where the prediction for $E_{cm} = 134$ GeV decreases faster than the power-like behaviour typical of QCD, and in the range of negative η (the photon is coming from the right, as in the HERA conventions). By construction, there is no dynamical information on the hard scattering process in the Weizsäcker-Williams approximation, which is simply a weighted sum of γp cross sections; this is also clear from the shape of the solid curves in fig. 1. For this reason, in this section we will mainly consider monochromatic photon-proton collisions at $E_{cm} = 268$ GeV. We have verified that our conclusions apply down to the lowest center-of-mass energies relevant at HERA.

We now turn to the problem of studying the reliability of the perturbative expansion. To this purpose, we have considered photon-proton collisions at 268 GeV as a representative case and we have computed various distributions, varying factorization and renormalization scales by a factor of 2 around our default choice, as customary in QCD in order to assess the magnitude of the neglected higher-order corrections. QCD predictions for photon-hadron cross sections are computed in terms of two distinct components: the so-called pointlike component, in which the photon directly interacts with partons in the hadron, and the hadronic component, in which the photon fluctuates into hadronic states, which subsequently interact with the hadron. This distinction is well defined at leading order, but becomes arbitrary when higher order

terms in the perturbative expansion are included (we will thoroughly discuss this problem in the following). Explicitly, the cross section is written as

$$d\sigma_{\gamma p}(K_\gamma, K_p) = d\sigma_{\gamma p}^{\text{point}}(K_\gamma, K_p) + d\sigma_{\gamma p}^{\text{hadr}}(K_\gamma, K_p) \quad (2.4)$$

where

$$d\sigma_{\gamma p}^{\text{point}}(K_\gamma, K_p) = \sum_j \int dx f_j^{(p)}(x, \mu'_H) d\hat{\sigma}_{\gamma j}(K_\gamma, xK_p, \alpha_s(\mu'_R), \mu'_R, \mu'_H, \mu_\gamma), \quad (2.5)$$

$$d\sigma_{\gamma p}^{\text{hadr}}(K_\gamma, K_p) = \sum_{ij} \int dx dy f_i^{(\gamma)}(x, \mu_\gamma) f_j^{(p)}(y, \mu''_H) \\ \times d\hat{\sigma}_{ij}(xK_\gamma, yK_p, \alpha_s(\mu''_R), \mu''_R, \mu''_H, \mu_\gamma), \quad (2.6)$$

and $f_i^{(p)}(f_i^{(\gamma)})$ are the distribution functions of parton i inside the proton (photon). $d\hat{\sigma}_{\gamma j}$ and $d\hat{\sigma}_{ij}$ are the subtracted short-distance partonic cross sections, which are finite at any order in perturbative QCD. The dependence of $d\sigma_{\gamma p}^{\text{point}}$ on μ'_R, μ'_H , and of $d\sigma_{\gamma p}^{\text{hadr}}$ on μ''_R, μ''_H , cancels in each component separately, up to NNLO terms. On the other hand, the dependence on μ_γ in $d\sigma_{\gamma p}^{\text{point}}$ is compensated by the analogous dependence in $d\sigma_{\gamma p}^{\text{hadr}}$ (see for example ref. [19] for a detailed discussion on this point). In the language of Altarelli-Parisi equations, the collinear singularities of the photon leg in the pointlike component are re-absorbed (at a scale μ_γ) in the parton densities of the photon entering the hadronic component.

We begin by studying single-inclusive quantities and two-jet observables, defined with $E_{1T}^{\text{cut}} \neq E_{2T}^{\text{cut}}$. We set all the scales in eqs. (2.5) and (2.6) to the same value, which we denote by μ , and we study the dependence of the physical quantities upon μ . In this case, this procedure gives a good estimate of the full uncertainty affecting the results, which in principle should be obtained by considering independent variations of all the scales. In the left plot of fig. 2 we present the distribution in the pseudorapidity of jets with $E_T > E_T^{\text{cut}}$, for $E_T^{\text{cut}} = 10$ GeV and 20 GeV. In the right plot of the same figure we show the distribution in the invariant mass of the two hardest jets, for $E_{1T}^{\text{cut}} = 10$ GeV, $E_{2T}^{\text{cut}} = 15$ GeV (upper curves) and $E_{1T}^{\text{cut}} = 20$ GeV, $E_{2T}^{\text{cut}} = 25$ GeV (lower curves). The jets are defined by the cone algorithm with $R = 1$. The scale dependence is moderate, and slightly reduces with increasing transverse energy cuts. We checked that other kinematical quantities, like the E_T of the jet, the pseudorapidity of the pair, the difference in rapidity of the pair, show a similar scale dependence. From the left-hand side of fig. 2, we see that the scale dependence of the pseudorapidity

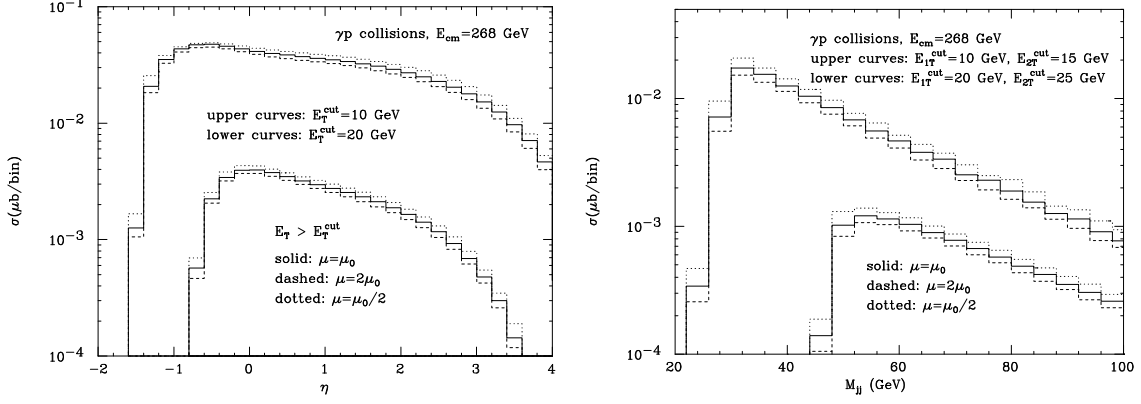


Figure 2: Scale dependence of the single-inclusive jet pseudorapidity and two-jet invariant mass distributions, for different values of the minimum allowed transverse energy of the observed jets.

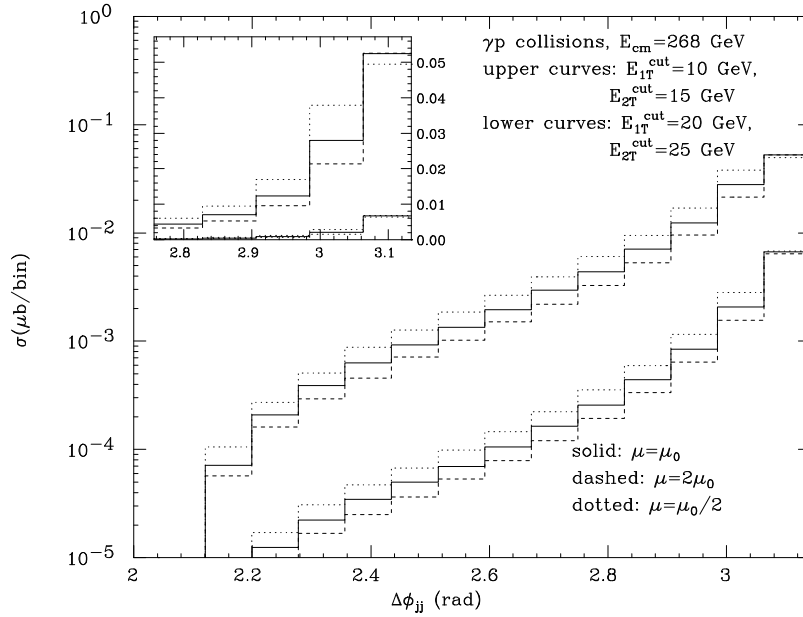


Figure 3: Scale dependence of the azimuthal distance distribution in two-jet events, for different values of the minimum allowed transverse energy of the two hardest jets ($E_{1T}^{\text{cut}} \neq E_{2T}^{\text{cut}}$).

distribution is slightly stronger for η values which are far from the central region. This is what we expect, since large η values correspond to small transverse energies, and therefore to less reliable QCD predictions.

We also computed the same quantities for a cone with an opening angle of $R = 0.7$. In this case, the scale dependence of both the pseudorapidity and the invariant mass distributions is slightly reduced.

The situation is different for the azimuthal correlation $\Delta\phi_{jj}$ between the two jets with largest transverse momenta, shown in fig. 3. For $\Delta\phi_{jj} < \pi$ the two sets of curves corresponding to the different choices of transverse momentum cuts show the same scale dependence, larger than in the case of pseudorapidity and invariant mass distributions of fig. 2. This is due to the fact that the $\Delta\phi_{jj}$ correlation is a pure NLO effect in this region. The scale dependence reduces for $\Delta\phi_{jj} \simeq \pi$, as can be also seen from the small inserted figure.

The $\Delta\phi_{jj}$ correlation computed with a cone of $R = 0.7$ shows the same scale dependence as in the case $R = 1$ for $\Delta\phi_{jj} < \pi$, and a stronger scale dependence for $\Delta\phi_{jj} \simeq \pi$.

We now consider the problem of computing two-jet inclusive quantities for $E_{1T}^{cut} = E_{2T}^{cut} \equiv E_T^{cut}$. As far as infrared safeness is concerned, there is nothing special in this choice. The cross section is well-defined and finite at any order in perturbation theory. On the other hand, there are quantities which at next-to-leading order display a pathological behaviour. This can be seen very easily by studying the inclusive two-jet total cross section

$$\sigma_2(\Delta) = \sigma(E_{1T} > E_T^{cut}, E_{2T} > E_T^{cut} + \Delta) \quad (2.7)$$

for $\Delta \rightarrow 0$. The next-to-leading order QCD results are shown in fig. 4, where we have chosen $E_T^{cut} = 10$ GeV and $E_T^{cut} = 20$ GeV (the curve for $E_T^{cut} = 20$ GeV has been rescaled by a factor of 11 in order to make both curves visible on the same plot). Notice that the value of $\sigma_2(\Delta)$ for $\Delta = 0$ is finite, as expected for an infrared-safe quantity. Observe also, on the other hand, that $\sigma_2(\Delta)$ has an infinite slope in $\Delta = 0$. This fact can be understood in the following way. We consider the real emission contribution when one of the emitted partons is quasi-collinear to one of the initial state partons (at NLO in QCD this implies that the two jets are identified with the

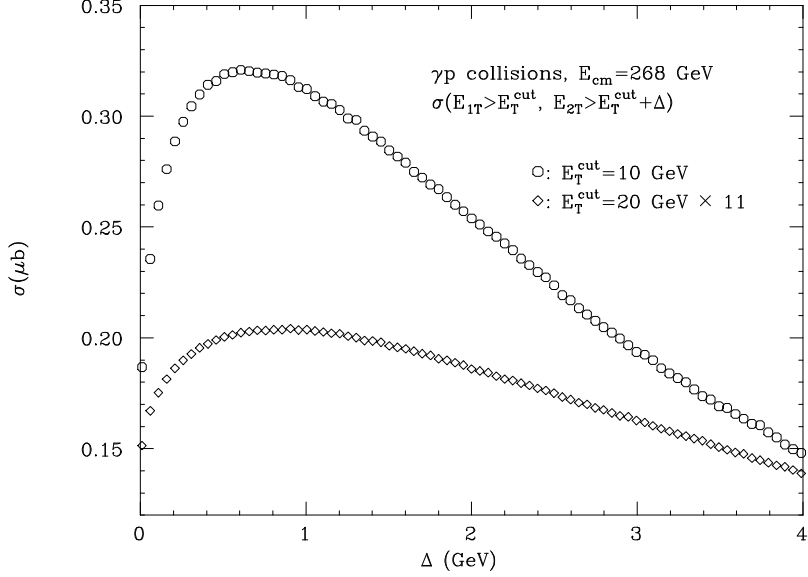


Figure 4: *Inclusive two-jet total cross section for $E_{1T} > E_T^{cut}$ and $E_{2T} > E_T^{cut} + \Delta$, as a function of Δ , for two different values of E_T^{cut} .*

two other partons). The leading collinear singularity of this contribution is given by

$$\sigma^{(r)} = \int d^2 p_{1T} \theta(E_{1T} - E_T^{cut}) \int d^2 p_{2T} \theta(E_{2T} - E_T^{cut} - \Delta) \frac{1}{|\vec{p}_{1T} + \vec{p}_{2T}|^2 + \delta}, \quad (2.8)$$

where δ acts as a collinear cutoff. The integral can be easily computed, and we get

$$\sigma^{(r)} = A(\Delta, \delta) + B \log \delta - C \cdot (\Delta + \delta) \log(\Delta + \delta), \quad (2.9)$$

where both $A(\Delta, \delta)$ and its first derivative with respect to Δ are regular in $\Delta = 0$ for any δ , including $\delta = 0$, and C is a positive coefficient. The term $B \log \delta$ is the genuine collinear singularity, and it is cancelled by the corresponding singular terms in the two-body contribution. For fixed $\Delta \neq 0$, one can safely take $\delta = 0$ in the last term. For $\Delta \rightarrow 0$ this term vanishes, but its first derivative with respect to Δ diverges, and this is the origin of the behaviour observed in the full calculation, shown in fig. 4. Alternatively, one could have started with $\Delta = 0$, as we did for the distributions shown in fig. 1. In this case, the last term in eq. (2.9) becomes $\delta \log \delta$, which vanishes for $\delta \rightarrow 0$, although less rapidly than terms linear in δ . Because of this extra δ dependence, the $\Delta = 0$ case is a reason of concern [8] when the calculation is performed with a technique which requires keeping $\delta \neq 0$, as for example the slicing

method. We remark that in the subtraction method the introduction of the non-physical parameter δ is avoided, and therefore the $\Delta = 0$ case does not require any special care.

One striking feature of fig. 4 is that $\sigma_2(\Delta)$ is not a monotonically decreasing function for increasing Δ , as one might expect on the basis of simple phase-space considerations. This behaviour is also present in our simple model, eq. (2.9), because of the negative sign in front of last term. This effect is induced by the truncation of the perturbative series at NLO. Roughly speaking, at this order there is not enough emission of soft real gluons to compensate for the large negative contribution of the soft-virtual terms. We therefore expect quantities like $\sigma_2(\Delta)$ to be poorly predicted by NLO QCD for $\Delta = 0$. However, the mismatch between virtual and real contributions is effective only in some special regions of the phase space; typical examples are the threshold of the invariant mass of the pair and the region around $\Delta\phi_{jj} = \pi$ in the azimuthal distance correlation of the two hardest jets. It is well known that fixed-order perturbation theory is not reliable in these regions, and that resummation of all-order contribution is needed. Despite this fact, the cross section is expected to be well-behaved in the remaining part of the phase space.

In the following, we will show that two-jet inclusive distributions can be safely studied even in the case of equal transverse energy cuts on both jets. To address this issue, we performed a more careful study of the scale dependence of the results. In particular, we varied independently μ_γ and $\mu_R = \mu_H$, where $\mu_R = \mu'_R$ and $\mu_H = \mu'_H$ when we consider the pointlike component, eq. (2.5), while $\mu_R = \mu''_R$ and $\mu_H = \mu''_H$ when we consider the hadronic component, eq. (2.6). We also verified that independent variations of μ_R and μ_H would not modify our conclusions. We begin with the $\Delta\phi_{jj}$ correlation, shown in fig. 5. The region $\Delta\phi_{jj} < \pi$ does not pose any problem, being a pure NLO effect. For this reason, the curves were calculated again with $\mu_\gamma = \mu_R = \mu_H$. As in the case $E_{1T}^{cut} \neq E_{2T}^{cut}$, no improvement in the scale dependence is seen when transverse energy cuts are increased. The small inserted figure shows the region $\Delta\phi_{jj} \simeq \pi$; in this case, the curves have been evaluated by varying the scales independently. In the bin around $\Delta\phi_{jj} = \pi$ the curves corresponding to $E_T^{cut} = 10$ GeV show a very strong scale dependence, thus signalling a failure of the perturbative expansion in this region. Notice also that most of the uncertainty band in the last bin gives negative cross sections. By considering independent scale variations, this band increases of about 25% with respect to the case when all the scales are set to the same value. When E_T^{cut} is increased to 20 GeV, this effect is more moderate, but

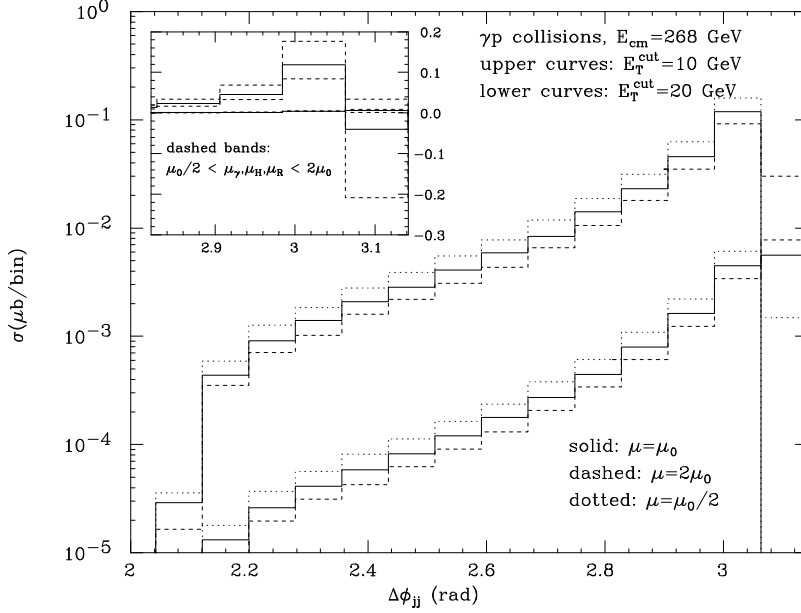


Figure 5: *Scale dependence of the azimuthal distance distribution in two-jet events, for different values of the minimum allowed transverse energy of the two hardest jets ($E_{1T}^{cut} = E_{2T}^{cut} = E_T^{cut}$).*

the scale dependence is still larger than in the region $\Delta\phi_{jj} < \pi$ (this is consistent with fig. 4, where we see that the total cross section decreases faster for $\Delta \rightarrow 0$ in the case of smaller transverse momentum cuts, thus indicating that in this case soft gluon emission is more important). We expect that an all-order resummation would have a moderate impact in this case. Of course, the above considerations are partially dependent on the chosen bin size: enlarging the bin around $\Delta\phi_{jj} = \pi$ enough, the perturbative prediction becomes reliable for any choice of E_T^{cut} .

We now turn to the distribution of the invariant mass of the pair. This distribution is non-trivial already at leading order, and therefore, in principle, the effect of soft gluon emission is not confined in some particular region of the phase space. To clearly show the effect of an independent variation of the scales, we separately present in fig. 6 the pointlike and the hadronic contributions, for the choice $E_{1T}^{cut} = E_{2T}^{cut} = 10$ GeV. The solid curves are the defaults, the dotted (dashed) curves are obtained by varying $\mu_R = \mu_H$ (μ_γ). We see that the pointlike and the hadronic component display opposite behaviours with respect to the scale μ_γ (for $\mu_\gamma = 2\mu_0$, the curve is larger than the default one for the hadronic component, and smaller for the pointlike component).

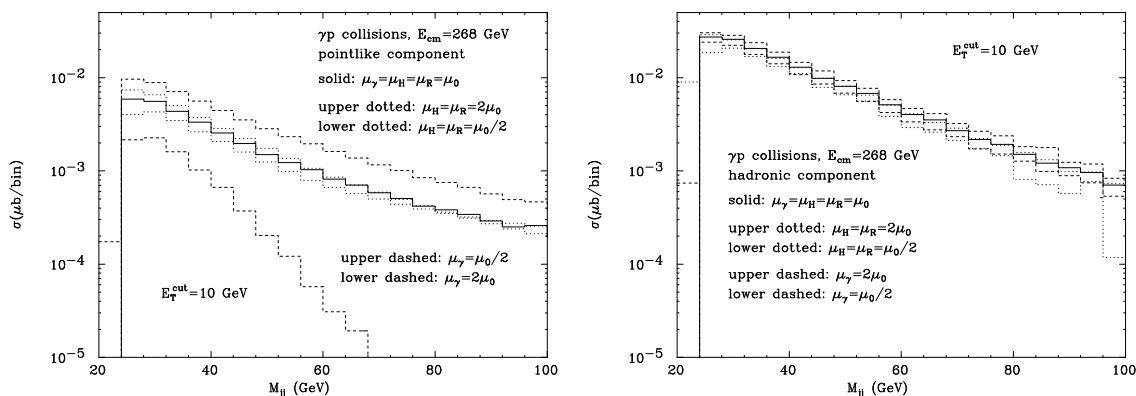


Figure 6: *Scale dependence of the invariant mass distribution in two-jet events. The pointlike (left) and hadronic (right) components are separately shown ($E_{1T}^{cut} = E_{2T}^{cut} = E_T^{cut}$).*

This shows the cancellation mechanism between eqs. (2.5) and (2.6). In particular, the fact that the hadronic component is larger than the pointlike one implies that a moderate μ_γ dependence in the hadronic contribution induces a huge μ_γ dependence in the pointlike contribution, as can be seen from fig. 6. This does not mean that the prediction of the theory is not reliable: in fact, the only measurable quantity is the sum of the two components, shown in fig. 7. From that figure, we see that the compensation between the μ_γ dependence of the two components is remarkable, and the residual dependence is rather small. On the other hand, there is no cancellation mechanism in the case of the μ_R and μ_H dependence, since these quantities are different in the pointlike and hadronic components (see eqs. (2.5) and (2.6)). The corresponding uncertainties must be summed incoherently. Nevertheless, these uncertainties are small, therefore resulting in a small uncertainty on the physical result, fig. 7.

This discussion does not apply to the region where M_{jj} is close to the threshold. From fig. 7 we see that the bin around $M_{jj} = 20$ GeV shows a large scale dependence, and that some of the curves are negative. In this region, the perturbative expansion therefore breaks down, like in the case $\Delta\phi_{jj} \simeq \pi$ we discussed above.

We conclude that NLO QCD provides reasonably stable predictions for jet production at HERA. Single-inclusive variables are very well described. In the case of two-jet inclusive quantities, we have to distinguish the cases $E_{1T}^{cut} \neq E_{2T}^{cut}$ and $E_{1T}^{cut} = E_{2T}^{cut}$. In the former case, the perturbative result is rather accurate, and gives reliable predic-

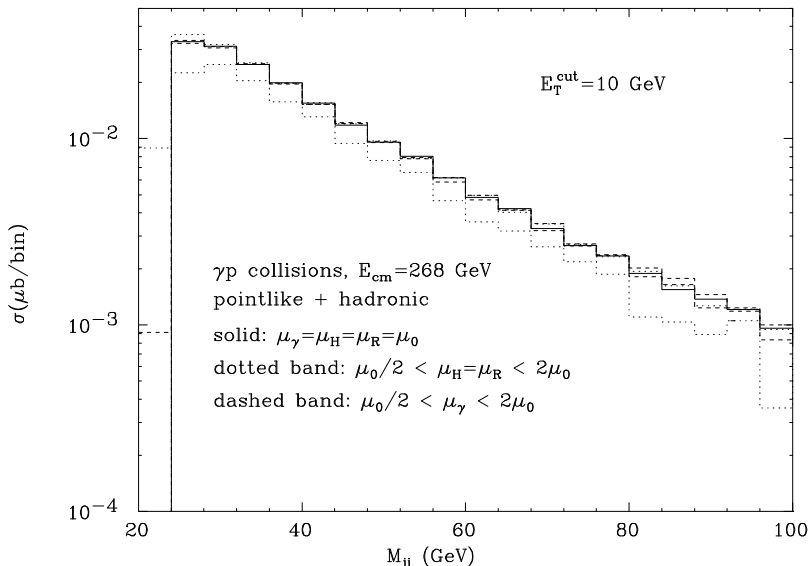


Figure 7: *Scale dependence of the invariant mass distribution in two-jet events ($E_{1T}^{\text{cut}} = E_{2T}^{\text{cut}} = E_T^{\text{cut}}$).*

tions in the full range of any quantity (this assumes that E_{1T}^{cut} and E_{2T}^{cut} are not too close to each other. By inspection of fig. 4, it is safe to take $|E_{1T}^{\text{cut}} - E_{2T}^{\text{cut}}| > 2$ GeV). In the latter case, there are regions of the phase space which are particularly sensitive to soft gluon emission, and therefore require an all-order resummation. In these regions ($\Delta\phi_{jj} \simeq \pi$, $p_T^{jj} \simeq 0$, M_{jj} close to the threshold) the fixed-order QCD results are not reliable, and no significant comparison can be made with experimental results (which, on the other hand, can be safely obtained, since $E_{1T}^{\text{cut}} = E_{2T}^{\text{cut}}$ does not imply infrared non-safeness). Elsewhere, two-jet correlations can be predicted to a level of accuracy comparable to the one obtained in the case $E_{1T}^{\text{cut}} \neq E_{2T}^{\text{cut}}$.

As discussed above (see in particular fig. 6) the pointlike and hadronic components are strongly correlated in perturbative QCD beyond leading order. This issue is interesting in the light of the fact that some analyses of experimental data are performed with specific kinematical cuts, imposed in order to measure physical quantities which are supposed to be dominated by the pointlike or the hadronic component of the cross section for any reasonable scale choice. In jet physics, such cuts are usually defined in terms of the variable

$$x_\gamma = \frac{E_{1T}e^{-\eta_1} + E_{2T}e^{-\eta_2}}{2E_\gamma}, \quad (2.10)$$

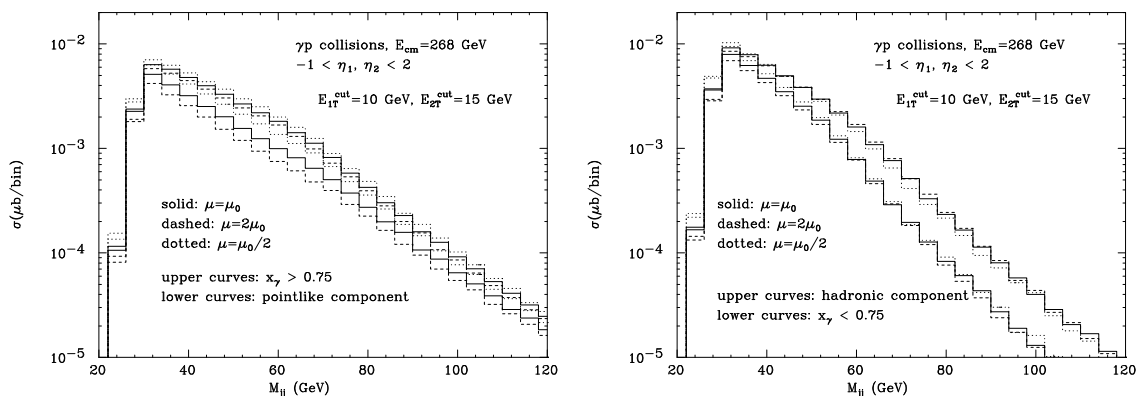


Figure 8: Scale dependence of the invariant mass distribution, for $x_\gamma > 0.75$ (left) and $x_\gamma < 0.75$ (right), compared with the pointlike and hadronic component respectively.

where E_{iT} and η_i ($i = 1, 2$) are the transverse energies and pseudorapidities of the two hardest jets in the event. For two-jet production at leading order, x_γ is equal to 1 for the pointlike component (in the hadronic component x_γ is the fraction of the photon longitudinal momentum carried by the interacting parton). At higher orders, this identification no longer holds, but one might expect that the high- x_γ region is dominated by the pointlike component, and the low- x_γ region by the hadronic one. Following this criterion, in some analyses the pointlike (hadronic) component is *operationally* defined as the measured cross section for x_γ larger (smaller) than some fixed value, usually 0.75. With such a definition, one might for example hope to pose direct constraints on the parton densities in the photon, or to get information on the details of the underlying parton dynamics, using jet data.

In order to assess the effectiveness of this procedure, we have computed the pair invariant mass distribution imposing the cuts $x_\gamma > 0.75$ or $x_\gamma < 0.75$. We considered again γp collisions at a center-of-mass energy of 268 GeV, defining the jet by the cone algorithm with $R = 1$. In fig. 8 we present our results for the choice $E_{1T}^{cut} = 10$ GeV, $E_{1T}^{cut} = 15$ GeV. In the figure on the left (right), we show our prediction for the curve with $x_\gamma > 0.75$ ($x_\gamma < 0.75$), together with the pointlike (hadronic) component. As before in the case $E_{1T}^{cut} \neq E_{2T}^{cut}$, the scale dependence has been studied by setting all the scales to the same value. The cuts $-1 < \eta_1, \eta_2 < 2$ have been imposed on the pseudorapidity of the two observed jets in order to simulate a realistic geometrical acceptance. We observe that the hadronic component (see fig. 8 right) is sizeably

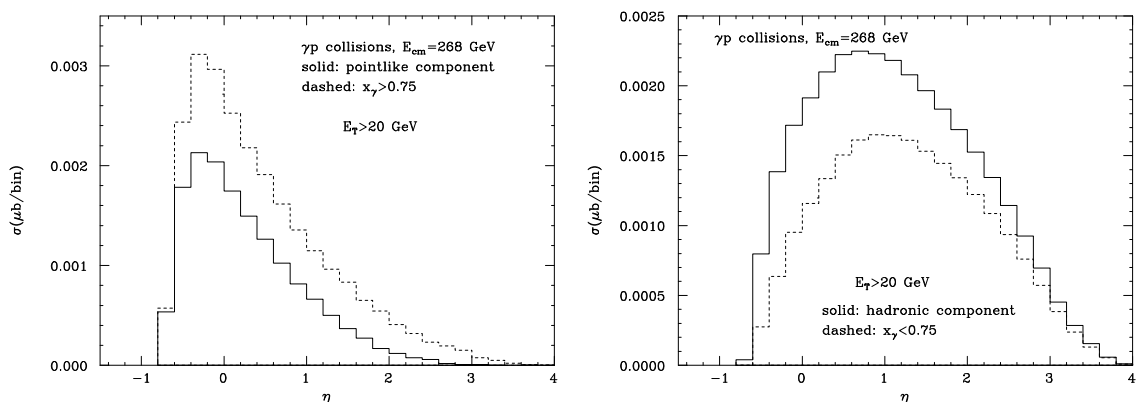


Figure 9: *Pseudorapidity distribution for $x_\gamma > 0.75$ (left) and $x_\gamma < 0.75$ (right), compared with the pointlike and hadronic component respectively. The scales have been set to the default value.*

larger than the distribution for $x_\gamma < 0.75$. This implies that in the region $x_\gamma < 0.75$ the pointlike and the hadronic contributions mix significantly for any scale choice. The same pattern is displayed by the pointlike component and the distribution for $x_\gamma > 0.75$ (fig. 8 left); in this case the scale dependence of the pointlike component is somewhat larger. We also computed the distributions of fig. 8 in the case $E_{1T}^{cut} = E_{2T}^{cut} = 10$ GeV. We observe the same behaviour; the difference between the hadronic (pointlike) component and the curve for $x_\gamma < 0.75$ ($x_\gamma > 0.75$) is even larger than that shown in fig. 8.

We found that the mixing between the hadronic and pointlike components is sizeable for all the physical observables, even in simple cases like single-inclusive distributions. As an example, we present in fig. 9 the comparison between the hadronic (pointlike) component of the η distribution, and the corresponding curve obtained with a $x_\gamma < 0.75$ ($x_\gamma > 0.75$) cut. Although in this case the shapes are quite similar, the absolute normalization is rather different. We have checked that the difference between the two curves in each plot of fig. 9 is larger than the corresponding scale uncertainty.

This discussion suggests that, because of the effect of radiative corrections, a cut at $x_\gamma = 0.75$ is probably not very useful to distinguish between partonic subprocesses with or without an incoming photon. Nevertheless, it is still conceivable that by cutting in x_γ , one may select observables which are particularly sensitive to the parton

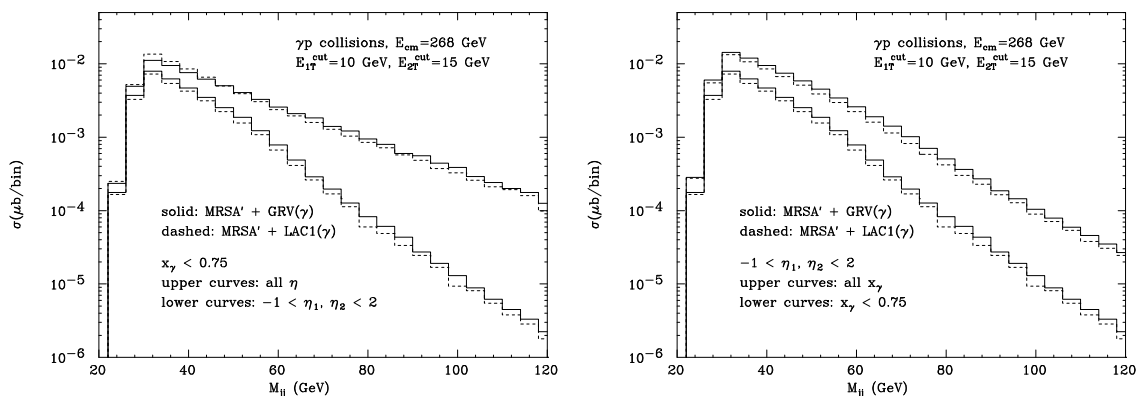


Figure 10: *Dependence of the invariant mass distribution upon the parton densities in the photon.*

densities in the photon. In order to further investigate this issue, we have computed the invariant mass distribution for $x_\gamma < 0.75$ with rather an extreme choice of the parametrization of parton densities in the photon, namely the LAC1 [20] set, and compared it to our previous results obtained with the GRV-HO set. The invariant mass is particularly suitable to this purpose, since it is directly related to the Bjorken- x region probed in the collision (for a given center-of-mass energy, small invariant masses correspond to the small- x region). One can see from fig. 10 that the difference between the results obtained with the GRV and LAC1 sets is comparable to the uncertainty band induced by the scale variations we discussed above. In the central pseudorapidity region the sensitivity to the different parametrizations is very small. In particular, the right plot of fig. 10 shows that in this η region the x_γ cut does not enhance the dependence upon the photon parton densities. Notice that fig. 10 is relevant for monochromatic photon-proton collisions at $E_{cm} = 268$ GeV; for smaller center-of-mass energies or for electron-proton collisions in the Weizsäcker-Williams approximation the sensitivity is even more suppressed, because larger values of the Bjorken- x are probed. The main difference between the GRV and LAC1 sets is in the behaviour of the gluon density at small x . To effectively probe this region at HERA smaller values of the invariant mass must be chosen, and QCD predictions become less reliable.

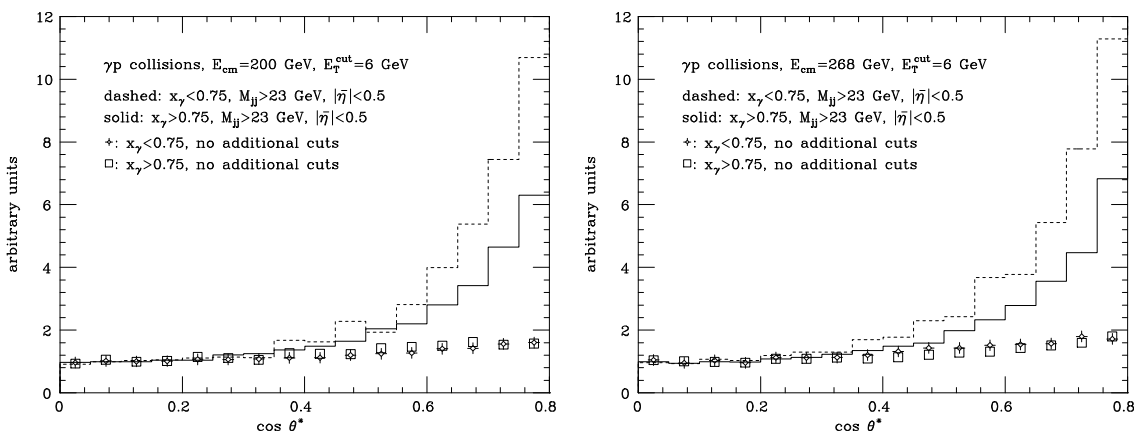


Figure 11: *Distribution in $\cos \theta^*$, for γp collisions and various kinematical cuts ($E_{1T}^{cut} = E_{2T}^{cut} = E_T^{cut}$).*

3. Phenomenology of jet production at HERA

In this Section we will discuss the predictions of perturbative QCD for some quantities of phenomenological interest. We begin by considering the distribution in the variable $\cos \theta^*$, defined as

$$\cos \theta^* = \tanh \frac{|\eta_1 - \eta_2|}{2}, \quad (3.1)$$

where $\eta_{1,2}$ are, as before, the pseudorapidities of the two hardest jets. In QCD at leading order the hadronic component is predicted to behave as $(1 - |\cos \theta^*|)^{-2}$ when $\cos \theta^* \rightarrow 1$, as opposed to the $(1 - |\cos \theta^*|)^{-1}$ behaviour of the pointlike component. It is interesting to check whether the measured distributions for $x_\gamma < 0.75$ and $x_\gamma > 0.75$ display a similar behaviour. In fig. 11 we present the $\cos \theta^*$ distribution in γp collisions for $E_{1T}^{cut} = E_{2T}^{cut} = 6$ GeV, for two different center-of-mass energies. We see that for both values of E_{cm} the curves for $x_\gamma > 0.75$ and $x_\gamma < 0.75$, represented in fig. 11 by squares and crosses respectively, have approximately the same shape (the two curves have been normalized to have the same integral in the first four bins, in order to compare the shapes). This confirms the expectations of the previous section, where we have shown that distributions in the $x_\gamma < 0.75$ (or $x_\gamma > 0.75$) region are the result of a significant mixing between the hadronic and the pointlike components. It is interesting to notice that a difference in the behaviour at $\cos \theta^* \sim 1$ of the two distributions obtained for $x_\gamma < 0.75$ and $x_\gamma > 0.75$ can be induced by other

kinematical cuts. To show this, we have computed the $\cos \theta^*$ distribution in the two x_γ regions, applying the cuts $M_{jj} > 23$ GeV and $|\bar{\eta}| < 0.5$, with $\bar{\eta} = (\eta_1 + \eta_2)/2$. These are the same cuts adopted by the ZEUS collaboration in the analysis of ref. [21]. This curves (normalized as before to the same integral in the first four bins) are also shown in fig. 11; we see that the curves for $x_\gamma < 0.75$ (dashed) and $x_\gamma > 0.75$ (solid) display a different behaviour for $\cos \theta^* \rightarrow 1$; this difference is generated by the introduction of the kinematical cuts. This effect can be understood observing that

$$M_{jj}^2 = 2E_{1T}E_{2T} [\cosh(\eta_1 - \eta_2) - \cos \Delta\phi_{jj}]. \quad (3.2)$$

Large values of the invariant mass correspond therefore to large values of $\cosh(\eta_1 - \eta_2)$; on the other hand,

$$\cosh(\eta_1 - \eta_2) = \frac{1 + \cos^2 \theta^*}{1 - \cos^2 \theta^*}. \quad (3.3)$$

It is clear from eq. (3.3) that a large- M_{jj} cut enhances the region $\cos \theta^* \sim 1$. This shows that the difference in shape between the solid and dashed curves in fig. 11 is not directly related to a different dynamical production mechanism. The curve corresponding to $x_\gamma < 0.75$ has a steeper rise basically because the invariant mass distribution relevant for this x_γ region is softer than the invariant mass distribution for $x_\gamma > 0.75$. One may then argue that this is still a signal of different production mechanisms. But, as we discussed in the previous section, the mixing between the pointlike and the hadronic components is especially relevant in the case of $E_{1T}^{cut} = E_{2T}^{cut}$, and therefore no particularly significant information on the parton dynamics can be extracted from the invariant mass distribution with a x_γ cut.

For a given observable, the largest statistics will be collected by integrating over the energies of the incident photons. For this reason, we will now present predictions obtained for jet production in ep collisions in the Weizsäcker-Williams approximation, with $E_{cm}(ep) = 300$ GeV, $Q^2 = 0.01$ GeV² and $0.2 \leq y \leq 0.8$ (see eqs. (2.1) and (2.2)). In order to perform a realistic study, we will apply kinematical cuts which approximately reproduce the experimental conditions of the HERA experiments. The pseudorapidity of the observed jets will be restricted in the range $-1 < \eta < 2$. In the case of two-jet quantities, we will require $E_{1T}^{cut} = 11$ GeV and $E_{2T}^{cut} = 14$ GeV. By definition, the two jets are always the hardest of the event.

As discussed in the previous section, with this choice of cuts on transverse energies we expect the perturbative expansion to be well-behaved over the whole phase space. For this reason, we study the scale dependence of our results by setting all the scales to

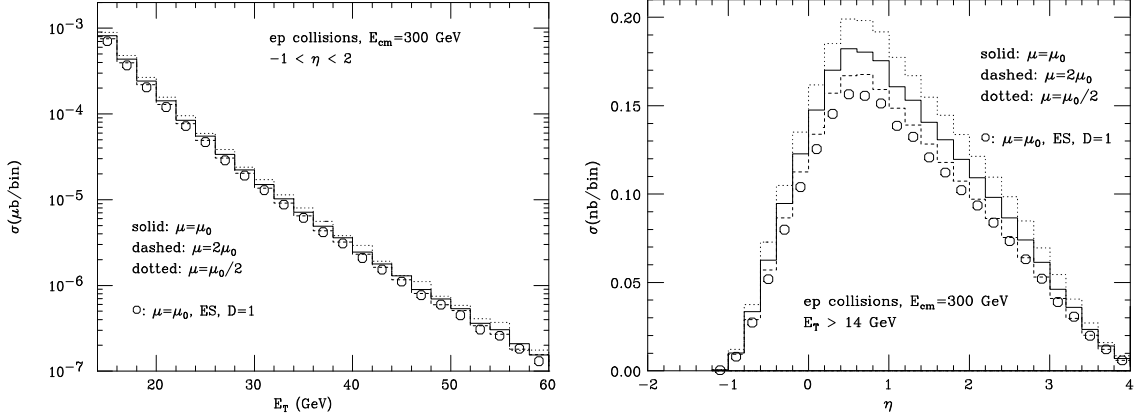


Figure 12: *Single-inclusive transverse energy and pseudorapidity. Jets are defined by the cone algorithm (solid curves; the scale dependence is also shown) and by the prescription of ref. [22] (circles).*

the same value μ . We present predictions obtained with two different jet definitions, namely the cone algorithm, with $R = 1$, and the algorithm proposed by Ellis and Soper in ref. [22], with $D = 1$. In the case of the cone algorithm we show the full scale variation computed as before, while for the Ellis-Soper algorithm we only present the predictions corresponding to our central scale choice. We recall that a modification of the standard cone algorithm has been introduced in ref. [23] to improve the comparison with data; this modification however would not change our conclusions, and we will use $R_{sep} = 2R$ in the following.

In fig. 12 we show single-inclusive distributions in transverse energy and pseudorapidity of the jet (in the latter case, we require the jet to have transverse energy larger than 14 GeV). In fig. 13 and fig. 14 we show two-jet correlations which are non-trivial at leading order: the invariant mass of the pair, the absolute value of the difference in pseudorapidity of the two observed jets, and the average pseudorapidity of the pair, $\bar{\eta} = (\eta_1 + \eta_2)/2$; notice that the latter quantity is equal, at leading order, to the rapidity of the pair. Finally, fig. 15 shows correlations trivial at leading order, the transverse momentum of the pair and the azimuthal distance. This set of observables gives a fairly complete description of the production mechanism; it is clearly possible to consider even more exclusive quantities, by imposing additional kinematical cuts.

The results presented in figs. 12, 13 and 14 display a remarkable stability with respect to scale choice. The difference between the default curve (solid histogram)

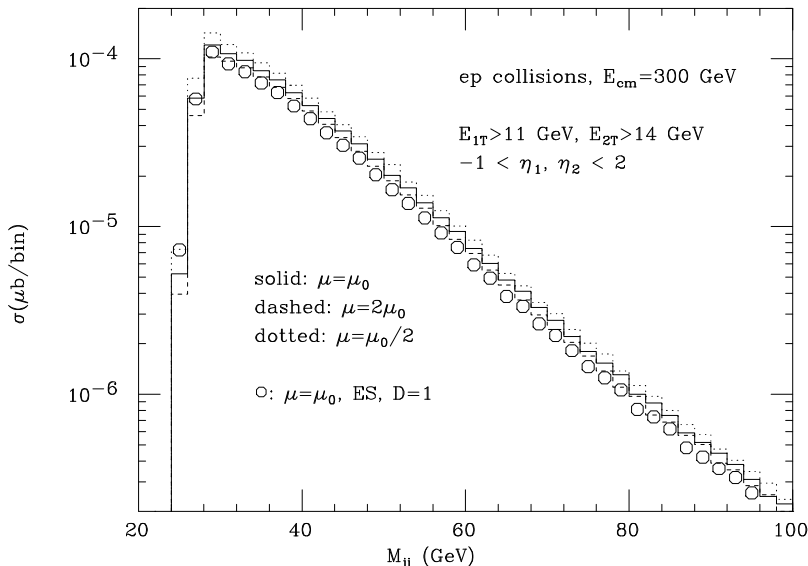


Figure 13: *Invariant mass of the pair of jets with the largest transverse momenta. Jets are defined by the cone algorithm (solid curve; the scale dependence is also shown) and by the prescription of ref. [22] (circles).*

and the curves corresponding to $\mu = 2\mu_0$ and $\mu = \mu_0/2$ (dashed and dotted histograms respectively) is about 10%. We remark that the non-logarithmic term in the Weizsäcker-Williams function, eq. (2.1), gives a negative contribution of the order of 7% with $Q^2 = 0.01 \text{ GeV}^2$, and of 5% with $Q^2 = 4 \text{ GeV}^2$, and is therefore non-negligible. Using the jet definition of ref. [22], represented by circles, one gets shapes similar to the ones given by the cone algorithm with $R = 0.7$.

Consistently with what we found in the previous section, the scale dependence is larger in the case of the plots of fig. 15, which are a pure next-to-leading order effect except for the bins around $p_T^{jj} = 0$ and $\Delta\phi_{jj} = \pi$. In this case, differences of about 25% are induced by scale variations. The distributions obtained with the Ellis-Soper algorithm are broader than those obtained with the cone algorithm and $R = 1$, when the jets tend to be more back-to-back in the transverse plane.

We have also checked that the choice of parton densities does not influence the QCD predictions very much. For example, using the MRS125 set, characterized by the fact that $\alpha_s(m_Z)$ is fixed to the value 0.125, the shape of the distributions does not change, and the modification in the overall normalization is easily traced back to

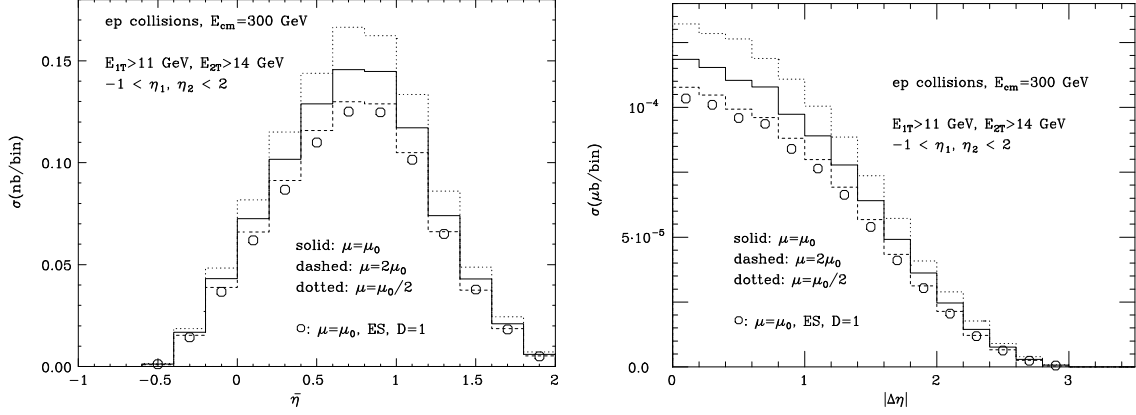


Figure 14: *Average pseudorapidity and difference in pseudorapidity of the pair of jets with the largest transverse momenta. Jets are defined by the cone algorithm (solid curves; the scale dependence is also shown) and by the prescription of ref. [22] (circles).*

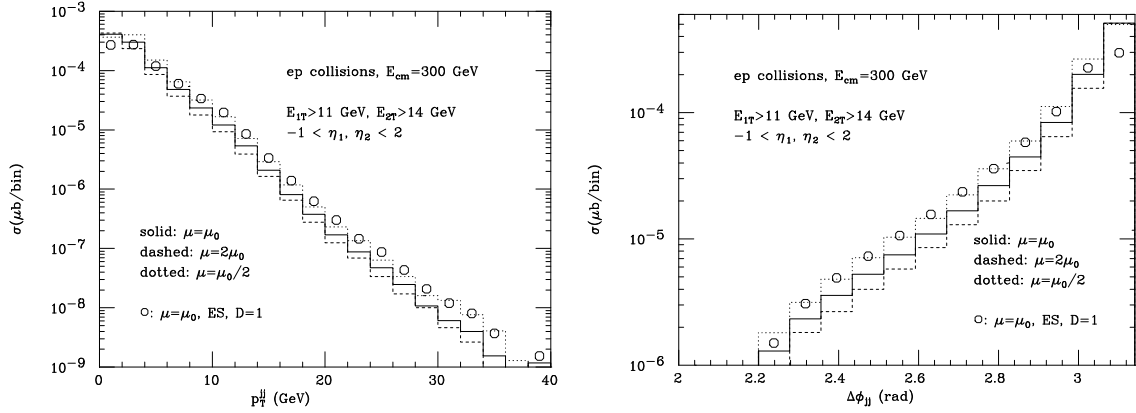


Figure 15: *Transverse momentum and azimuthal correlation of the pair of jets with the largest transverse momenta. Jets are defined by the cone algorithm (solid curves; the scale dependence is also shown) and by the prescription of ref. [22] (circles).*

the different value of α_S .

4. Conclusions

In this paper we have studied the phenomenology of jet photoproduction at HERA at next-to-leading order in QCD. We used the subtraction method, which does not require an approximate expression for the matrix elements and the introduction of non-physical infrared cutoffs which are necessary in other approaches (like the slicing method). We found that, starting from transverse energy scales of the order of 10 GeV, the theoretical predictions are sufficiently stable with respect to scale variation to allow for a significant comparison with high-statistics data. In some cases, like two-jet inclusive quantities defined with equal cuts on the transverse energy of the observed jets, the next-to-leading order result turns out to be unreliable in some special regions of the phase space, corresponding typically to configurations in which the jets are back-to-back in the transverse plane, or to the threshold of the invariant mass distribution. In these cases, an all-order resummation would be needed to get a consistent result. On the other hand, in the remaining part of the phase space the next-to-leading order result is well-behaved, and meaningful comparisons with experimental data can be carried out.

We have considered the problem of the separation of the pointlike and the hadronic components of the cross sections. This task could in principle be performed, if a suitable operational definition could be given for the two components (the pointlike and hadronic components defined as in eqs. (2.5) and (2.6) are not physical observables beyond leading order). We found that by cutting in the variable x_γ , defined with the two hardest jets of a given event, the operationally defined pointlike or hadronic components are actually a sizeable mixture between the next-to-leading order pointlike and hadronic cross sections, for any reasonable choice of scales. This implies that this kind of cut is not very useful to extract information on the underlying parton dynamics. Also, at the transverse energy scales where the perturbative expansions is reliable, the sensitivity of the operationally defined hadronic component to the parton densities in the photon is rather limited.

Finally, we have considered a sample set of one-jet and two-jet inclusive observables which can be measured in order to have a detailed description of the production mechanism. We have computed these quantities in the Weizsäcker-Williams approximation, applying a set of realistic cuts in order to reproduce the experimental analyses of the HERA experiments. We found that the results are remarkably stable with respect to scale variation, and therefore that the measurements of these quantities could

be used as a quality test of perturbative QCD.

Acknowledgements

One of us (GR) thanks the Institute of Theoretical Physics of ETH, Zurich, for the kind hospitality. We thank C. Grab, Z. Kunszt, H. Niggli, P. Nason and S. Passaggio for many interesting discussions. We are indebted to Tancredi Carli, Costas Foudas and Amedeo Staiano for providing us with useful information about experimental analyses.

References

- [1] F. Aversa, M. Greco, P. Chiappetta and J. P. Guillet, *Z. Phys.* **C46**(1990)253;
Phys. Rev. Lett. **65**(1990)401;
S. D. Ellis, Z. Kunszt and D. E. Soper, *Phys. Rev. Lett.* **64**(1990)2121;
Phys. Rev. Lett. **69**(1992)1496;
W. T. Giele, E. W. N. Glover and D. A. Kosower, *Phys. Rev. Lett.* **73**(1994)2019;
S. D. Ellis and D. E. Soper, *Phys. Rev. Lett.* **74**(1995)5182.
- [2] G. Sterman and S. Weinberg, *Phys. Rev. Lett.* **39**(1977)1436;
R. K. Ellis, D. A. Ross and A. E. Terrano, *Nucl. Phys.* **B178**(1981)421;
Z. Kunszt and P. Nason, in *Z Physics at LEP 1*, eds. G. Altarelli, R. Kleiss and C. Verzegnassi, Geneva, 1989;
G. Kramer and B. Lampe, *Fortschr. Phys.* **37**(1989)161;
S. Bethke, Z. Kunszt, D. E. Soper and W. J. Stirling, *Nucl. Phys.* **B370**(1992)310;
W. T. Giele and E. W. N. Glover, *Phys. Rev.* **D46**(1992)1980;
S. Catani and M. H. Seymour, *Phys. Lett.* **B378**(1996)287;
A. Signer and L. Dixon, *Phys. Rev. Lett.* **78**(1997)811, [hep-ph/9609460](#);
preprint SLAC-PUB-7528, [hep-ph/9706285](#).
- [3] CDF Coll., F. Abe *et al.*, *Phys. Rev. Lett.* **68**(1992)1104; *Phys. Rev. Lett.* **77**(1996)438.
- [4] H. L. Lai *et al.*, *Phys. Rev.* **D55**(1997)1280, [hep-ph/9606399](#).

- [5] CDF Coll., F. Abe *et al.*, *Phys. Rev. Lett.* **70**(1993)1376;
see also P. Melese, for the CDF Coll., preprint FERMILAB-CONF-97-167-E,
presented at 11th Les Rencontres de Physique de la Vallée d’Aoste, La Thuile,
Italy, 2-8 Mar 1997.
- [6] L. E. Gordon and J. K. Storrow, *Phys. Lett.* **B291**(1992)320;
D. Bödeker, *Z. Phys.* **C59**(1993)501;
G. Kramer and S. G. Salesh, *Z. Phys.* **C61**(1994)277;
D. Bödeker, G. Kramer and S. G. Salesh, *Z. Phys.* **C63**(1994)471;
M. Klasen and G. Kramer, *Z. Phys.* **C72**(1996)107, [hep-ph/9511405](#).
- [7] M. Klasen and G. Kramer, preprint DESY 96-246, [hep-ph/9611450](#).
- [8] B. W. Harris and J. F. Owens, preprint FSU-HEP-970411, [hep-ph/9704324](#).
- [9] S. Frixione, preprint ETH-TH/97-14, [hep-ph/9706545](#).
- [10] J. M. Butterworth, for the H1 and ZEUS Coll., preprint UCL/HEP 97-04, pre-
sented at the Ringberg Workshop, Tegernsee, 25-30 May 1997, [hep-ex/9707001](#).
- [11] P. Aurenche, preprint ENSLAPP-A-652-97, talk given at Photon 97, Egmond
aan Zee, Netherlands, 10-15 May 1997, [hep-ph/9706386](#).
- [12] S. Frixione, Z. Kunszt and A. Signer, *Nucl. Phys.* **B467**(1996)399, [hep-ph/9512328](#).
- [13] C.F. Weizsäcker, *Z. Phys.* **88**(1934)612; E.J. Williams, *Phys. Rev.* **45**(1934)729.
- [14] V.M. Budnev *et al.*, *Phys. Rev.* **C15**(1974)181;
H.A. Olsen, *Phys. Rev.* **D19**(1979)100.
- [15] S. Frixione, M. Mangano, P. Nason and G. Ridolfi, *Phys. Lett.* **B319**(1993)339.
- [16] F. Aversa *et al.*, Proceedings of the Summer Study on High Energy Physics,
Research Directions for the Decade, Snowmass, CO, Jun 25 - Jul 13, 1990.
- [17] A. D. Martin, R. G. Roberts and W. J. Stirling, *Phys. Lett.* **B354**(1995)155,
[hep-ph/9502336](#).
- [18] M. Glück, E. Reya and A. Vogt, *Phys. Rev.* **D46**(1992)1973.
- [19] S. Frixione, M.L. Mangano, P. Nason and G. Ridolfi, *Nucl. Phys.* **B412**(1994)225.

- [20] H. Abramowicz, K. Charchula and A. Levy, *Phys. Lett.* **B269**(1991)458.
- [21] M. Derrick *et al.*, ZEUS Coll., *Phys. Lett.* **B384**(1996)401, [hep-ex/9605009](#).
- [22] S. D. Ellis and D. E. Soper, *Phys. Rev.* **D48**(1993)3160.
- [23] S. D. Ellis, Z. Kunszt and D. E. Soper, *Phys. Rev. Lett.* **69**(1992)3615.